arXiv:0711.4122v1 [cond-mat.mtrl-sci] 26 Nov 2007

A simple and efficient model for mesoscale solidification simulation of globular grain structures

Stéphane Vernède[1,2], Michel Rappaz[1]

12 october 2006

[1] Computational Materials Laboratory,
Ecole Polytechnique Fédérale de Lausanne,
Station 12, Lausanne, CH-1015 Switzerland

[2]Alcan-CRV,
ZI Centr'alp, 0725 rue Aristide Berges,
BP 27, Voreppe, FR-38341 France

keywords: solidification, equiaxed microstructure, modelling, surface energy

Published in Acta Materialia, Volume 55, Issue 5, March 2007, Pages 1703-1710
view at publisher

Abstract

A simple model for the solidification of globular grains in metallic alloys is presented. Based on the Voronoi diagram of the nuclei centers, it accounts for the curvature of the grains near triple junctions. The predictions of this model are close to those of more refined approaches such as the phase field method, but with a computation cost decreased by several orders of magnitude. Therefore, this model is ideally suited for *granular simulations* linking the behavior of individual grains to macroscopic properties of the material.

1 Introduction

Microstructures that form during solidification of metallic alloys play a key role for the final properties of as-cast materials and for subsequent heat treatments. They also condition the formation of defects such as porosity and hot cracking [1]. As solidification of one or more solid phases is a moving free-boundary problem, several techniques have been developed especially over the past decade to overcome the difficulty of tracking the solid-liquid interface.

One of the most powerful and widely used methods is the phase field technique [2]. In this method, the sharp interface is replaced by a continuous field varying from 0 in the solid to 1 in the liquid with a diffuse interface over a finite thickness. As the phase field method is based on thermodynamics considerations, it provides a unified framework for many phenomena (formation of dendrites, eutectics, peritectics, etc.). Yet, this method is very computation intensive as the mesh size has to be small with respect to the diffuse interface thickness, and the diffuse interface thickness has to be small with respect to the typical radius of curvature of the microstructure (e.g., dendrite tip radius, eutectic spacing). Moreover, since the problem is generally solved using an explicit scheme, a Fourier criterion must be satisfied to ensure numerical stability. This is why nowadays, phase field simulations are limited to the simulation of a few grains, very often in two dimensions. Other techniques such as the level set [3] or pseudo-front tracking [4] methods have been developed, with different advantages and drawbacks, but they roughly require the same amount of computations.

If fundamental aspects of microstructure formation can be tackled with such sophisticated methods, it must also be recognized that there is an increasing need for simulations that can relate microstructure and macroscopic properties. This is particularly important for the last stage of solidification, during which the most important defects (porosity, hot tears) form. In particular, the gradual topological transition of the microstructure from continuous liquid films to a continuous and fully coherent solid is essential for hot tearing. Because of the random nature of nucleation, this transition is associated with the formation of increasingly larger clusters of grains as described by the percolation theory [5]. Therefore, the mechanical properties and feeding ability of the mushy zone during this transition cannot be deduced from the morphology of just a few grains [6].

In order to study the gradual formation of a coherent solid phase in globular alloys, an original approach has been proposed by Mathier et al. [7]. In this model, grains are approximated by polyhedrons based on the Voronoi diagram of a random set of nuclei. In order to compute the solidification of large and non-isothermal mushy zones, Vernède et al. further simplified the assumptions of this model [8]. Yet, these two approaches lead to polyhedral grains and cannot account for the formation of isolated liquid pockets at the triple junctions of the grains.

In the present contribution, a solidification model based on the approach of Mathier et al. but accounting for the Gibbs-Thomson effect near grain corners is described. The predictions of this model are shown to be close to those obtained with more refined methods such as the phase field or pseudo-front tracking methods, but with a computation time several orders of magnitude lower. After a brief recall of the *granular model* of solidification based on the Voronoi tessellation, the account of the Gibbs-Thomson effect and its implementation in the model are described. In the last section, simulation results are compared with those obtained with a pseudo-front tracking method, thus providing a basis of discussion for setting up bonds to this simple approach.

2 A solidification model based on Voronoi diagrams

This 2 dimensional solidification model has been derived first by Mathier et al. [7] and further developed by Vernède et al. [8]. For a better understanding the main lines of this model are recalled here.

The model assumes simultaneous nucleation of grains in a plane with a given density of random sites. Further assuming that the temperature difference across the average grain size is small with respect to the undercooling (i.e., small thermal gradient), the final grain

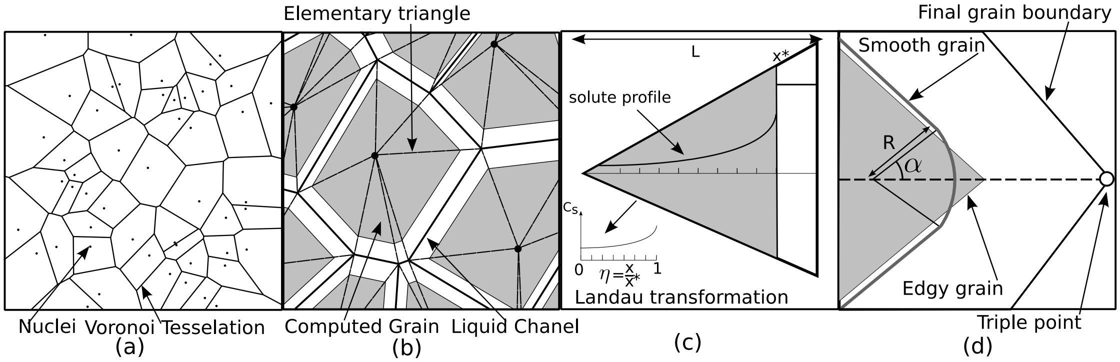

Figure 1: Various enlargements of the granular model: Voronoi tessellation associated with the nuclei centers (a); shape of the grains during solidification (b); solute balance within one triangle (c); smoothing procedure of the solid-liquid interface near the grain corners (d).

structure is close to the Voronoi tessellation of the set of nuclei (Fig. 1, (a)) [9]. In the present work, the Voronoi tessellation was computed using the free access software *qhull* [10].

In order to further simplify the solidification model, the solute flux between elementary triangles is neglected in a first step. Thus, the smooth interface of each grain during growth can be approximated by a linear segment in each triangle connecting the nucleation center with a Voronoi segment. By construction, these segments are perpendicular to the vectors connecting the nucleation centers and the two triangles issued from the same Voronoi segment are symmetrical, (Fig. 1, (b)).

Solidification is reduced therefore to a one-dimensional problem in each triangle, with the assumption of complete mixing of solute in the liquid phase and back-diffusion in the solid. Moreover, the temperature of the system is imposed, either uniform or given by a fixed thermal gradient and decreasing with a given cooling rate. Therefore, the solute balance integrated over the liquid phase of an elementary triangle gives:

$$x^* D_s \frac{\partial c_s^*}{\partial x}(x^*) + v^* x^* (k-1) c_\ell + \frac{1}{2}(L^2 - {x^*}^2)\frac{\partial c_\ell}{\partial t} = 0 \tag{1}$$

where x^* and v^* are the position and speed of the interface, respectively, c_s and c_ℓ the solute concentration in the solid and liquid phase, c_s^* the solute concentration in the solid at the interface, k the partition coefficient, t the time, D_s the diffusion coefficient in the solid, L the height of the elementary triangle perpendicular to the Voronoi segment and x the coordinate along this direction (Fig. 1, (c)). The last term of Eq. 1 accounts for the evolution of solute concentration, which is imposed by an external cooling rate $\dot{T}$ and the phase diagram. Thus

$$x^* D_s \frac{\partial c_s^*}{\partial x}(x^*) + v^* x^* (k-1) c_\ell + \frac{1}{2}(L^2 - {x^*}^2)\frac{\dot{T}}{m} = 0 \tag{2}$$

where m is the slope of the liquidus.

The first term in Eq. 2 associated with back-diffusion in the solid is computed by solving the cylindrical diffusion equation in the solid phase, which can be viewed as the solute balance between slices of the elementary triangle for constant x:

$$\frac{\partial c_s}{\partial t} = D_s \left(\frac{\partial^2 c_s}{\partial x^2} + \frac{1}{x}\frac{\partial c_s}{\partial x} \right) \tag{3}$$

In order to easily account for solidification, we use a Landau transformation of the solid domain [0,x*(t)] into the reference 1D domain [0,1], as introduced by Voller and Sundarraj [11]:

$$c_s(x,t) \rightarrow c_s(\eta,t) \quad \eta = \frac{x}{x^*} \tag{4}$$

Thus Eq. 3 becomes:

$$\left(\frac{\partial c_s}{\partial t}\right)_\eta = \frac{D_s}{x^{*2}}\frac{\partial^2 c_s}{\partial \eta^2} + \left(\frac{\eta v^*}{x^*} + \frac{D_s}{\eta x^{*2}}\right)\frac{\partial c_s}{\partial \eta} \tag{5}$$

where the term $\frac{\eta v^*}{x^*}$ accounts for the advection of the mesh with the solidification front. This equation is solved using a finite difference scheme, with a nil flux condition for $\eta = 0$ and an imposed concentration $c_s^* = kc_l$ for $\eta = 1$. Knowing the flux associated with back-diffusion and the concentration evolution in the liquid, the second term of Eq. 2 allows to deduce the velocity of the interface, v^*, and thus to find the new position $x^*(t + dt)$.

Note that solidification does not depend on the opening of the elementary triangles but only on its height L, i.e, on the half-distance between two nucleation centers. Near the end of solidification, the excess free energy needed to form a grain boundary out of two misoriented grains, i.e., coalescence undercooling [12], can be accounted for. This procedure is presented in Refs [7, 8] , but as this feature is not useful for the present contribution, it will not be detailed here.

3 A model for grain corners

Although the previous model predicts fairly well the evolutions of the grains, of the solid-liquid interface and of the solid fraction (see section 4), it leads to polyhedral grains (Fig. 1, (d)). This situation is clearly unrealistic as sharp corners are normally remelted by surface tension in non-faceted crystals. Furthermore, no liquid pocket can form at the triple junctions of the grains. As a consequence, this model overestimates the volume fraction of solid at which contact between grains occurs, as compared with experiments [8, 13].

In order to remove these limitations, the Gibbs-Thomson effect at grain corners has to be considered. Assuming again that temperature is homogeneous at the scale of a grain, the liquid concentration at an interface with a local radius of curvature R is given by:

$$c_\ell^R = c_\ell^\infty + \frac{\Gamma_{s\ell}}{Rm} \tag{6}$$

where c_ℓ^∞ is the liquid solute concentration for a flat interface and $\Gamma_{s\ell}$ is the Gibbs-Thomson coefficient. (Note that, in general, the liquidus slope m is negative). If solidification would be arrested, solute will flow from low curvature areas to high curvature areas, as for coarsening, thus remelting the highly curved zones. Yet, globular grains are not spherical during solidification and another phenomenon should balance the Gibbs-Thomson effect.

Therefore, the idealized situation represented in Fig. 2 is considered for smoothing the shape of polyhedral grains based on the Gibbs-Thomson effect. The grain corner is modelled by a curved interface with a constant radius of curvature R, whereas elsewhere the interface is supposed flat and parallel to the final grain boundary. Moreover, the liquid is divided

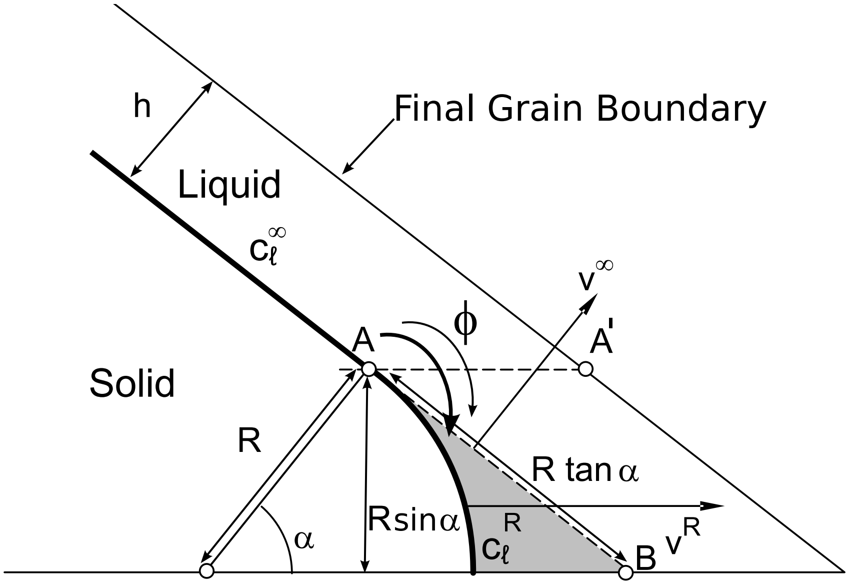

Figure 2: Schematics of the solute flux model which accounts for the Gibbs-Thomson effect near a grain corner.

into two zones, delimited by the dotted line AA' in Fig. 2. This line, passes through the point separating the flat and circular portions of the solid-liquid interface (point labelled A in Fig. 2). Close to the corner, the liquid has a concentration equal to c_ℓ^R, whereas in the second zone, surrounding the planar interface, a homogeneous concentration equal to c_ℓ^∞ is considered.

The gradient of solute around the corner can be estimated by $(c_\ell^R - c_\ell^\infty)/(R\sin\alpha)$ where $R\sin\alpha$ is the distance between the tips of the corner and limit of the two zones. Moreover, we consider that the flux of solute is effective over a length of the order of $R\sin\alpha$. This leads to an estimation of the overall flux flowing from the zone surrounding the flat interface to the zone surrounding the corner:

$$\Phi \sim D_\ell(c_\ell^\infty - c_\ell^R) = -\frac{D_\ell \Gamma_{s\ell}}{mR} > 0 \tag{7}$$

We further look for a radius of curvature that is stable with time , i.e., $\dot{R} = 0$. This implies that the limit between the curved and planar interface stays along the dotted line AA' in Fig 2. Once this constrain is fixed, it can be shown that the rejection of solute associated with a flat interface moving at a velocity v^∞ is equal to that rejected by the projection of the curved interface moving at a velocity v^R. Indeed, the projection of the curved interface is given by $R\sin\alpha$, whereas the velocity is given by $v^R = v^\infty/\cos\alpha$. So one has:

$$v^\infty R\tan\alpha = R\sin\alpha v^R = R\sin\alpha\frac{v^\infty}{\cos\alpha} \tag{8}$$

where $R\tan\alpha$ is the length of the extended flat interface (dotted line AB in Fig. 2). However, the grey surface is an additional volume of liquid, compared to the flat interface, and represents the advantage of the corner for solute diffusion. In other words, the small incoming flux of solute contributes to increasing the concentration of the liquid in the area, S, of the grey zone. A more rigorous development, based on solute balances, is given in Appendix. But in summary, one has:

$$\Phi = \frac{dc_\ell^R}{dt} S = \frac{dc_\ell^\infty}{dt} S = \frac{\dot{T}}{m} S = \frac{\dot{T}}{m} \frac{R^2}{2} (\tan\alpha - \alpha) \tag{9}$$

Combining Eq. 7 and 9, one finally gets:

$$R^3 = A_C \frac{2}{\tan\alpha - \alpha} \frac{\Gamma_{s\ell} D_\ell}{-\dot{T}} \tag{10}$$

where A_C is a dimensionless constant, arising from the simple description of the solute distribution (see Eq. 7). Nonetheless, simply setting its value to 1 produce satisfying results and this value will be used hereafter.

It is interesting to note at this stage that Eq. 10 is close to a coarsening law: the radius of curvature of a grain corner is proportional to the third power of a driving force given by $\frac{\Gamma_{s\ell} D_\ell}{\Delta T_o}$, where ΔT_o is the solidification interval of the alloy, and to the third power of the solidification time, t_f. The geometrical factor in front of this term is such that the radius of curvature becomes infinite when α is equal to 0 (the grain corner is flat) and nil when α is equal to $\frac{\pi}{2}$ (the grain has disappeared).

Using this relationship for the radius of curvature of the grain corners, the shape of the solid-liquid interface can be computed as follows.

- The position of the flat interface or solid fraction is computed for each elementary triangle using the back-diffusion model described above
- The radius of curvature at each grain corner is computed using Eq. 10. Please note that, for a fixed cooling rate, the radius is constant and can be computed only once before the time stepping procedure.
- The interface in each elementary triangle is approximated by a flat portion and two rounded corners. If the length of the flat interface becomes negative, the interface is approximated by an arc of a circle.
- Rounded interfaces increase the overall volume of liquid by creating liquid pockets at grain corners. The position of the flat interface is then moved slightly forward in order to conserve the solid fraction computed with the flat interface method (see Fig. 1 (d)).

4 Validity and limits of the model

The predictions of the present model have been compared with those obtained with a pseudo front tracking method (PFT) [4]. In this technique, the fraction of solid within each cell of an hexagonal network is computed based on an explicit solute diffusion calculation. A layer of cells always separate the solid and liquid phases and the solute flux balance for such cells is converted into a solid fraction evolution. The position of the interface within these interfacial cells is computed using a piece-wise linear interface calculation (PLIC) algorithm [14]. Once the interface position within each interfacial cell is known, its curvature and the associated Gibss-Thomson effect are calculated using a distance-field method similar to level-set. This

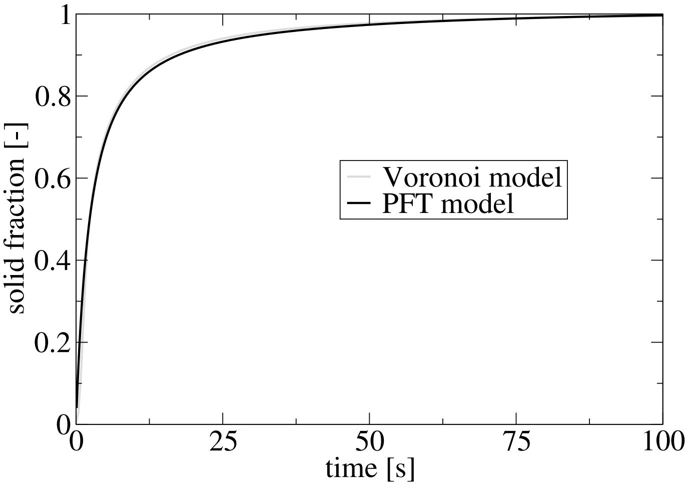

Figure 3: Solid fraction as a function of time computed with the Voronoi and the PFT methods

method leads to predictions close to the phase field method as shown in more details in Ref. [4].

The same simulations have been carried out with the PFT and the Voronoi methods. Six nuclei have been randomly placed in a $4.5 \cdot 10^{-2}$ mm^2 domain with periodic boundary conditions. The average grain size d_c is therefore around 90 μm. An Al-1wt%Cu has been considered with a linearised phase diagram ($m = -6.67$ K/wt% and $k = 0.14$). The other parameters used in these calculations are: $D_s = 1.5 \cdot 10^{-13}$ m^2/s, $D_\ell = 10^{-9} \cdot$ m^2/s, $\Gamma_{s\ell} = 5 \cdot 10^{-7}$ Km, $\dot{T}$ = -1 K/s.

Figure 3 shows the evolution of the solid fraction, g_s, computed with the two methods. Please keep in mind that, in the Voronoi method, the solid fraction calculated with rounded grains is equal to that obtained with polygonal grains. At the very beginning of solidification, grain growth predicted with the PFT method is slightly faster as the Voronoi method assumes complete mixing of solute in the liquid. As soon as a state of complete mixing is reached with the PFT method, the predictions of the two models are in very good agreement, even at high solid fraction. This shows that, despite the fairly strong assumptions of the (flat interface) Voronoi model, solute back-diffusion is well approximated.

In order to compare in more details the shape of the interfaces predicted by the two methods, the normalized specific solid liquid interface, S_s°, is represented in Fig 4 as a function of g_s. This dimensionless number corresponds to the total length of the solid-liquid interface of the grains divided by the number of grains and by the average final grain size d_c. This important parameter strongly influences the permeability of the grain assembly via the Carman-Kozeny relationship [15] as verified experimentally in aluminium alloys by Nielsen et al. [16]. A numerical study of S_s° also shows that this parameter is an indicator of the morphological transitions of the mushy zone [6]. As solid grains grow, the length of the solid liquid interface increases as $\sqrt{g_s}$ in 2D until impingement/contact of the solid grains makes it go to zero. Thus, S_s° is maximum when the new contacts between the grains counterbalance the natural increase of the interface length.

As can be seen on the left of Fig. 4, the overall shapes of $S_s^\circ(g_s)$ are in excellent agreement,

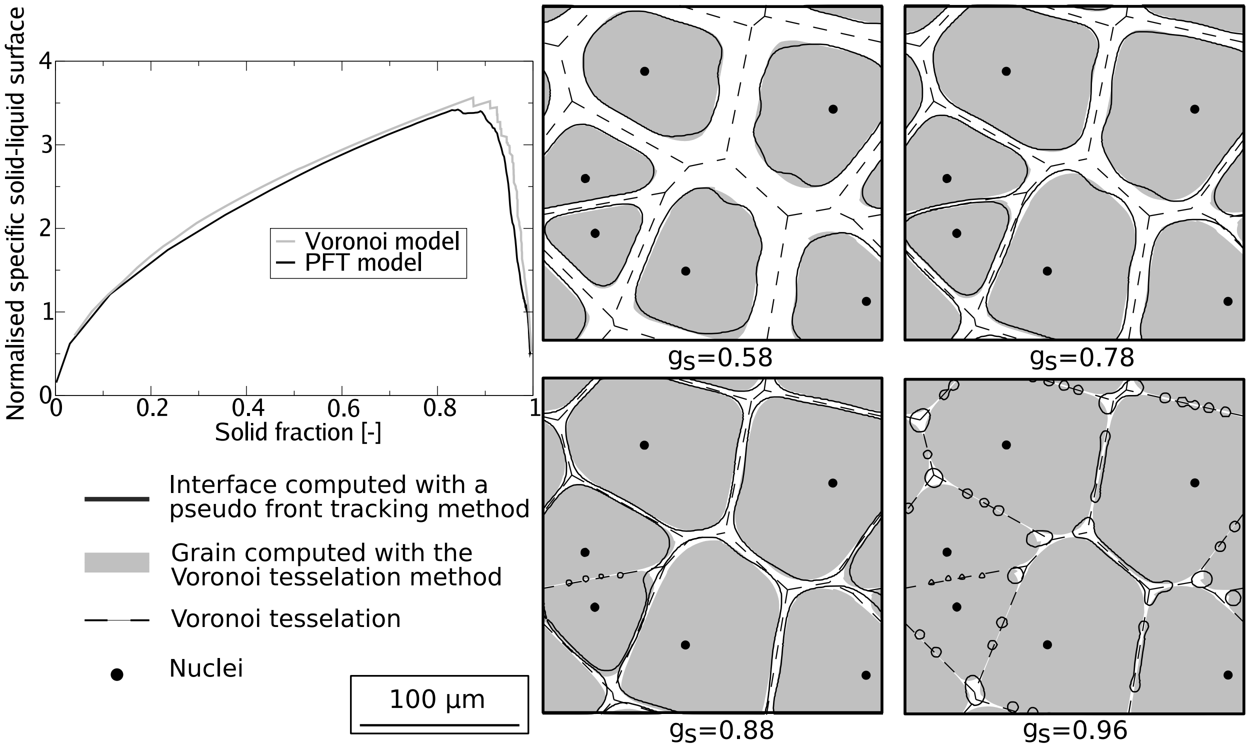

Figure 4: Comparison of the solid liquid interface shape predicted by the Voronoi and the PFT methods at various solid fractions.

but the Voronoi method slightly overestimates this parameter, thus revealing that grains are still slightly less rounded than those calculated with the PFT method. It should be specified that, under these conditions, the grains are clearly globular without significant destabilization of the interface. Formation of dendritic or globular dendritic grains would definitely increase the length of the solid-liquid interface, thus making $S^{\circ}_{s,PFT} > S^{\circ}_{s,Vor}$.

The grain shapes predicted by the two models at various solid fractions are also represented in Fig. 4. For visualization purpose, the grains computed by the Voronoi method are represented in grey, whereas the interfaces predicted by the PFT method are represented with black lines. Again, a fairly good agreement between the two simulations, especially near the grain corners, can be seen. Please note that interfaces predicted with the Voronoi model are not necessarily continuous as solidification is computed separately for each elementary triangle. Yet, these slight discontinuities do not affect much the topology of the liquid channel network, nor the estimation of the channels permeability and mushy zone topology.

The maximum of S°_{s} is predicted to occur at $g_s = 0.86$ by the PFT model, while it is delayed to $g_s = 0.89$ with the Voronoi model. This difference can be easily understood by looking at the shape of the grains at $g_s = 0.88$. With the PFT model, the liquid film in between two close neighboring grains can break down into small droplets by coalescence, whereas with the Voronoi model it remains a film until final impingement. Such a liquid film instability occurs when the grain boundary energy is lower than twice the solid-liquid interfacial energy, i.e., attractive boundaries, and the film thickness is on the order of the thickness of the diffuse solid-liquid interfaces.[12] No grain boundary energy has been set up in the PFT and Voronoi calculations, but the instability occurs too early with the PFT

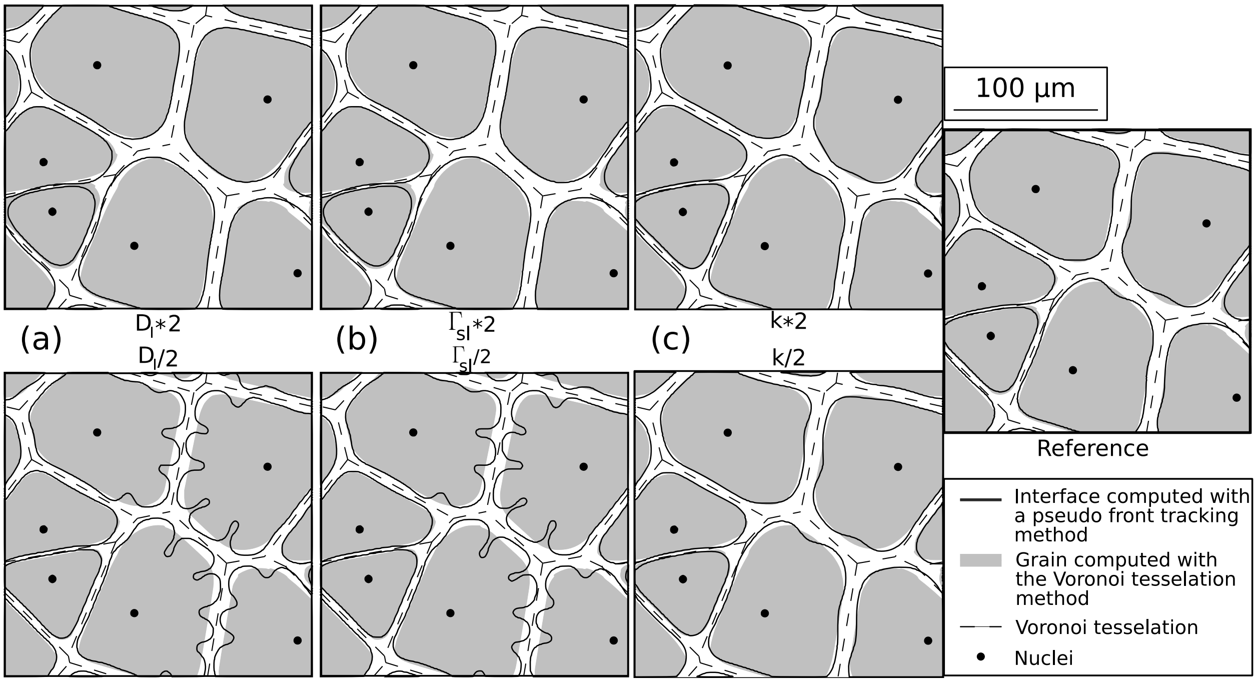
(a)
D_l*2
D_l/2
(b)
Γsl*2
Γsl/2
(c)
k*2
k/2
100 μm
Reference
Interface computed with a pseudo front tracking method
Grain computed with the Voronoi tesselation method
Voronoi tesselation
Nuclei

Figure 5: Comparison of grain shape at g_s=0.68 for various sets of solidification parameters. Starting from the reference simulation (right figure), one parameter is changed at a time: D_ℓ (a), $\Gamma_{s\ell}$ (b) and k (c) are multiplied (top) or divided (bottom) by 2 with respect to the reference.

method as it is conditioned by the mesh size rather than the diffuse interface thickness. Note that the quantitative simulation of the coalescence phenomenon remains a challenging topic despite advances done in the thermodynamic framework [12] and in the modelling of triple phase boundaries [17]. Please note also that grain boundary energies, and thus coalescence undercooling of repulsive interfaces, can be easily introduced in the present simulations.[8]

Despite the numerical difficulties associated with simulation of the last stage solidification, the radii of curvature at grain corners calculated with Eq. 10 are close to those arising from the complex PFT calculation, even for relatively narrow channels. After breakdown of the liquid films, the sizes of the liquid pockets at triple junction points are also in fairly good agreement. Note that the isolated liquid pocket are represented nevertheless with a negative curvature in the Voronoi simulation. It is clear that the rounding procedure does not account for the coalescence phenomenon which transforms globally convex globular grains into convex liquid pockets. This simplified approach nevertheless allows to introduce realistic volumes of liquid at triple junctions, thus decreasing the volume fraction of solid at which the flat portions of the grain interfaces impinge.

Figure 5 shows the effect of various parameters on the shape of the solid liquid interfaces. It is convenient to introduce a dimensionless number, C:

$$C = \frac{1}{d_c}\left(\frac{\Gamma_{s\ell} D_\ell}{(-\dot{T})}\right)^{\frac{1}{3}} \tag{11}$$

This number is the ratio of a ”typical” curvature radius at grains corner (i.e., when $(\tan\alpha - \alpha)^{-1} = 0.5$) and the average grain size. Figures 5 a) and b) show that a larger

C number corresponds indeed to a larger radius of curvature at grains corners, regardless whether this is achieved by increasing D_ℓ or $\Gamma_{s\ell}$. Moreover, the agreement between the PFT and Voronoi predictions remains when the physical parameters are changed. Yet, Fig. 5 also points out the limits of the present model, in particular at small C number. Indeed, the PFT predicts a destabilization of the globular grains into dendritic ones when C decreases. A criterion for the transition from globular to dendritic equiaxed grains has been recently proposed by Diepers et al.[18] These authors found that it occurs when:

$$d_c^{GD} = A_{GD}\left(\frac{L}{k\Delta T_o c_p}\frac{\Gamma_{s\ell}D_\ell}{(-\dot{T})}\right)^{\frac{1}{3}} \tag{12}$$

where c_p and L are the volumetric specific heat and latent of fusion, respectively, and A_{GD} a dimensionless factor function of the anisotropy of the solid-liquid interfacial energy. Although this criterion has been derived for a sphere and a cooling rate imposed only at the boundaries of the system, it is interesting to note that the same power-law of the ratio $\frac{D_\ell\Gamma_{s\ell}}{\dot{T}}$ is retrieved. The additional term,$(L/(k\Delta T_o c_p))$, comes from the solute undercooling ahead the solidification front and from an overall thermal balance. The destabilisation of the interface occurs at the beginning of solidification when this undercooling is crucial, whereas the selection of the grains corner curvature occurs latter in solidification when the solutal profile is flat. A change in the partition factor k, which does not affect the radius of curvature of the grains calculated with Eq. 10, nevertheless slightly influences the destabilization of the grains as predicted by Eq. 12 from the factor $k\Delta T_o$ and as observed with the PFT method (Fig. 5 c).

For a high C number, another limitation of the model is encountered as illustrated by the solidification of the smallest grain in Figs. 5 a) b). The Voronoi model does not predict well the solidification of this grain at high C number. This is because the overall curvature of the grain is not accounted for in the Voronoi method. Yet, the curvature undercooling during growth of globulitic grains remains very small, typically 0.01 K for a spherical grain of 20 μm radius. That of the last liquid droplets is slightly higher considering that the droplets are smaller and have a negative curvature, opposite to that considered here for the last liquid located at triple junctions. But in any case, curvature undercooling, despite its importance for coarsening and for the shape of the dendrite tip, is small in dendritic and globulitic solidification under normal conditions.

In order to use a Voronoi construction, e.g., linear grain boundaries, to predict the final grain structures, two assumptions have been made: first, the temperature is uniform at the scale of the grains, and second, the nuclei all start at the same time. The first hypothesis is usually verified for globulitic structures, e.g., grains of about 100 μm growing in a thermal gradient lower than 1 K/cm. The temperature difference across a reference specimen containing 100 grains is just 1 K in this case. The second hypothesis clearly pertains to alloys which are inoculated. It has been shown in the case of Al-alloys inoculated with TiB_2 particles that nucleation is athermal [19]. In athermal nucleation, the activation of a nucleant is a function of the undercooling only and not of time. In this case, the range of particle sizes which have been shown to be activated during solidification is typically 2-5 μm in diameter [19]. Therefore, the maximum nucleation undercooling is about 0.2 K for a Gibbs-Thomson coefficient of 10^{-7} Km. This value is small compared to the growth undercooling and thus an instantaneous nucleation assumption appears reasonable.

The most striking feature of the present Voronoi model is its low computation cost. The PFT simulations presented in Fig. 4 take around 12 Hours on a 2.8 GHz Pentium 4 personal computer, whereas the Voronoi calculations requires less than 2 s! This represents a gain of more than 4 orders of magnitude. This difference is even more striking with large mushy zones. The computation of a whole mushy zone solidification that contains 14000 grains (see Fig. 9 of Ref. [6]) requires less than 10 seconds on the same computer.

5 Conclusion

A model for the solidification of globular grains based on Voronoi diagrams and round corners has been derived. This model is shown to estimate well the shape of the globular grains during solidification and to take into account the effect of the various physical parameters, providing the interface does not become unstable. Its very low computation cost makes it an ideal base for granular simulation of mushy zone at a mesoscale, that can compute macroscopic properties such as mechanical properties or feeding properties based on the behaviour of individual grains [6]. Therefore, this model can be easily extended to 3 dimensions, providing new opportunities for realistic granular simulation.

6 Acknowledgement

This research is funded by Alcan CRV (France) and ANRT (Association Nationale de la Recherche Technique, France). The authors would like to thank Dr. A. Jacot from LSMX EPFL (Switzerland) for his help with the PFT simulations.

7 Appendix

Considering a section of the flat interface far from the corner, the speed of the interface can be estimated from the following flux balance.

$$h\frac{\partial c_\ell^\infty}{\partial t} = c_\ell^\infty(1-k)v^\infty - j_{bd}^\infty \tag{13}$$

The left hand term represents the variation of solute in the liquid, where h is the thickness of the liquid film. The first right hand term correspond to the solute rejected in the liquid due to the advance of the interface and j_{bd}^∞ is the flux pumped in the solid by back-diffusion. Similarly, a solute balance on the liquid part surrounding the corner (see main section) can be derived. If Ω denotes this domain, one has.

$$\int_\Omega \frac{\partial c_\ell}{\partial t} ds = c_\ell^R(1-k)R\sin\alpha v^R - \alpha R j_{bd}^R + \Phi \tag{14}$$

Please note that this balance accounts for the flux Φ exchanged between the flat and curved portions of the interface.

The variation of solute concentration at the interface is imposed by the cooling rate and $\partial_t c_\ell^\infty = \partial_t c_\ell^R = \dot{T}/m$. As a consequence, whatever is the precise repartition of solute around the grain corner, the variation of solute around the grain corner can be estimated by:

$$\int_\Omega \frac{\partial c_\ell}{\partial t} ds = S_\Omega \frac{\dot{T}}{m} \tag{15}$$

where S_Ω is the area of the domain surrounding the round corner. As $v^r = v^\infty / \cos\alpha$ (see main section), Eqs 13, 14 and 15 give:

$$S_\Omega \frac{\dot{T}}{m} = \frac{c_\ell^R}{c_\ell^\infty} R \tan\alpha (h \frac{\dot{T}}{m} + j_{bd}^\infty) - \alpha R j_{bd}^R + \Phi \tag{16}$$

Considering that $c_\ell^R / c_\ell^\infty \sim 1$ and neglecting the differences of back diffusion along the flat and curved parts of the interface, one gets:

$$(S + Rh\tan\alpha)\frac{\dot{T}}{m} = Rh\tan\alpha \frac{\dot{T}}{m} + \Phi \tag{17}$$

Where the surface S_Ω have been separated into the surface delimited by the extension of the flat interface ($Rh\tan\alpha$) and an extra surface S represented in grey in Fig. 2. As stated in the main part, one retrieve the fact that the solute rejected by the flat interface moving at velocity v^∞ is equivalent to that rejected by the curved interface moving at velocity $v^r = v^\infty / \cos\alpha$. Removing this term on the left and right hand sides finally gives:

$$S \frac{\dot{T}}{m} = \Phi \tag{18}$$

This represents the solute balance between the solute flux induced by the Gibbs-Thomson effect and the geometrical advantage of a corner for diffusion.

References

[1] J. Campbell. *Castings.* Butterworth Heineman, 1991.

[2] W. J. Boettinger, J. A.Warren, C. Beckermann, and A. Karma. Phase-field simulation of solidification. *Annu. Rev. Matter. Res.*, 32:163–94, 2002.

[3] Y.T. Kim, N. Goldenfeld, and J.A. Dantzig. Computation of dendritic microstructures using a level set method. *Phys. Rev. E*, 62(2):2471–74, 2000.

[4] A. Jacot and M. Rappaz. A pseudo-front tracking technique for the modelling of solidification microstructures in multi-component alloys. *Acta Mater.*, 50:1909–26, 2002.

[5] D. Stauffer and A. Aharony. *Introduction to percolation theory.* Taylor and Francis, 1994.

[6] S. Vernède, Ph. Jarry, and M. Rappaz. A granular model of equiaxed mushy zones: Formation of a coherent solid and localization of feeding. *Acta Mater.*, 54:4023–34, 2006.

[7] V. Mathier, A. Jacot, and M. Rappaz. Coalescence of equiaxed grains during solidification. *Mod. Sim. Mat. Sci. Eng.*, 12:479–490, 2004.

[8] S. Vernède and M. Rappaz. Transition of the mushy zone from continuous liquid films to a coherent solid. *Phil. Mag.*, 86(23):3779–94, 2006.

[9] Ch. Charbon and M. Rappaz. Shape of grain boundaries during phase transformations. *Acta Mater.*, 44:2663–68, 1996.

[10] C.B. Barber, D.P. Dobkin, and H.T. Huhdanpaa. The quickhull algorithm for convex hulls. *ACM Trans. of Mathematical Software*, 22:469–83, 1996.

[11] V.R. Voller and S. Sundarraj. *Mater. Sci. Tech.*, 9:474–481, 1993.

[12] M. Rappaz, A. Jacot, and W. Boettinger. Last stage solidification of alloys : Theorical model of dendrite arm and grain coalescence. *Met. Mater. Trans.*, 34A:467–479, 2003.

[13] I. Farup, J.M. Drezet, and M. Rappaz. In situ observation of hot tearing formation in succinonitrile-acetone. *Acta Mater.*, 49:1261–69, 2001.

[14] D.B. Kothe, W.J. Rider, S.J. Mosso, and J.S. Brock. Technical report, Los Alamos Research Laboratories, 1996.

[15] P.C. Carman. Fluid flow through granular beds. *Trans. Inst. Chem.*, 15:150, 1935.

[16] O. Nielsen, L. Arnberg, A. Mo, and H. Thevik. Experimental determination of mushy zone permeability in aluminum-copper alloys with equiaxed microstructures. *Met. Mater. Trans. A*, 30A:2455–62, 1999.

[17] R. Folch and M. Plapp. Quantitative phase-field modeling of two-phase solidification. *Phys. Rev. E*, 72(1):011602, 2005.

[18] H. J. Diepers and A. Karma. Globular-denditic transition in equiaxed alloy solidification. In *Solidification Processes and Microstructures.* M. Rappaz, Ch.Beckermann, R. Trivedi, (TMS Publ., Warrendale, PA, USA), 2004.

[19] T.E. Quested and A.L. Greer. Athermal heterogeneous nucleation of solidification. *Acta Mater.*, 53:2683–2692, 2005.